Published in final edited form as:

Circulation. 2008 June 24; 117(25): 3206–3215. doi:10.1161/CIRCULATIONAHA.107.757120.

Targeted Molecular Probes for Imaging Atherosclerotic Lesions With Magnetic Resonance Using Antibodies That Recognize Oxidation-Specific Epitopes

Karen C. Briley-Saebo, PhD, **Peter X. Shaw, PhD**, **Willem J.M. Mulder, PhD**, **Seung-Hyuk Choi, MD**, **Esad Vucic, MD**, **Juan Gilberto S. Aguinaldo, MD**, **Joseph L. Witztum, MD**, **Valentin Fuster, MD, PhD**, **Sotirios Tsimikas, MD***, and **Zahi A. Fayad, PhD***

Imaging Science Laboratory, Department of Radiology (K.C.B.-S., W.M., E.V., J.G.S.A., Z.A.F.) and Department of Cardiology, Zena and Michael A. Weiner Cardiovascular Institute, and Marie-Josee and Henry R. Kravis Cardiovascular Health Center (V.F., Z.A.F.), Mount Sinai School of Medicine, New York, NY; Vascular Medicine Program, University of California, San Diego (P.X.S., S.-H.C., J.L.W., S.T.); and Department of Medicine, Samsung Medical Center, Sungkyunkwan University School of Medicine, Seoul, Korea (S.-H.C.)

Abstract

Background—Oxidized low-density lipoprotein plays a key role in the initiation, progression, and destabilization of atherosclerotic plaques and is present in macrophages and the lipid pool. The aim of this study was to assess the feasibility of magnetic resonance imaging of atherosclerotic lesions in mice using micelles containing gadolinium and murine (MDA2 and E06) or human (IK17) antibodies that bind unique oxidation-specific epitopes.

Methods and Results—MDA2 micelles, E06 micelles, IK17 micelles, nonspecific IgG micelles, and untargeted micelles (no antibody) were prepared and characterized with respect to pharmacokinetics and biodistribution in wild-type and atherosclerotic apolipoprotein E–deficient (apoE$^{-/-}$) mice. Magnetic resonance imaging was performed at 9.4 T over a 96-hour time interval after the administration of 0.075–mmol Gd/kg micelles. MDA2, E06, and IK17 micelles exhibited a longer plasma half-life than IgG or untargeted micelles in apoE$^{-/-}$ but not wild-type mice. In apoE$^{-/-}$ mice, MDA2 and IK17 micelles showed maximal arterial wall uptake at 72 hours and E06 micelles at 96 hours, manifested by 125% to 231% enhancement in magnetic resonance signal compared with adjacent muscle. Confocal microscopy revealed that MDA2, IK17, and E06 micelles accumulated within atherosclerotic lesions and specifically within macrophages. Intravenous injection of free MDA2 before imaging with MDA2 micelles resulted in significantly diminished magnetic resonance signal enhancement. IgG micelles and untargeted micelles showed minimal enhancement in apoE$^{-/-}$ mice. There was no significant signal enhancement with all micelles in wild-type mice.

Correspondence to Zahi A. Fayad, Mount Sinai School of Medicine, Imaging Science Laboratory, One Gustave Levy Place, PO Box 1234, New York, NY 10029 (zahi.fayad@mssm.edu); or Sotirios Tsimikas, Vascular Medicine Program, University of California San Diego, 9500 Gilman Dr, La Jolla, CA 92993–0682 (stsimikas@ucsd.edu).

*The Fayad and Tsimikas laboratories contributed equally to this work.

Disclosures

Drs Tsimikas, Witztum, and Shaw are coinventors of patents owned by the University of California on the potential clinical use of oxidation-specific antibodies and have equity interest in Atherotope, Inc. The other authors report no conflicts.

Conclusions—Magnetic resonance imaging with micelles containing gadolinium and oxidation-specific antibodies demonstrates specific targeting and excellent image quality of oxidation-rich atherosclerotic lesions.

Keywords

Antibodies; atherosclerosis; inflammation; lipoproteins; magnetic resonance imaging

Atherothrombosis is a complex arterial disease in which cholesterol deposition, oxidation, extracellular matrix, chronic inflammation, and thrombus formation play major roles in mediating clinical sequelae.[1,2] It is now well established that plaque vulnerability is linked mainly to plaque composition and not necessarily to the degree of luminal narrowing.[3] Diagnostic tools that can accurately characterize plaque composition, particularly components that mediate the transition of stable plaques to vulnerable plaques, are needed to monitor disease, to assess the efficacy of therapeutic agents, and to predict cardiovascular events.[4]

Oxidized low-density lipoprotein (OxLDL) has been identified as a key factor in the initiation and progression of atherosclerosis in animal models and in the destabilization of vulnerable atherosclerotic plaques in humans.[5-7] Recent studies also have demonstrated that elevated levels of circulating oxidized phospholipids predict the presence and extent of angiographically defined coronary artery disease and the presence and progression of carotid and femoral artery atherosclerosis and predict death, myocardial infarction, and stroke in unselected populations from the general community.[8-10] Therefore, development of sensitive molecular imaging probes that target oxidation-specific epitopes in the vessel wall may allow in vivo detection of plaque vulnerability.

Because of its submillimeter resolution, magnetic resonance imaging (MRI) has emerged as a promising technique for both the direct assessment of plaque burden and the evaluation of plaque composition, particularly in large vessels.[11,12] The present study investigated the MRI efficacy of micelles loaded with gadolinium and the unique antibodies MDA2,[13] IK17,[14] and E06,[15] which recognize oxidation-specific epitopes, to image atherosclerotic lesions noninvasively.

Methods

Antibodies

MDA2 is a murine IgG monoclonal antibody that binds to malondialdehyde (MDA)-lysine epitopes present on modified LDL or other MDA-modified proteins.[13] MDA2 was generated with hybridoma technology and purified from ascites with a protein A column. IK17 is a fully human Fab fragment generated with phage-display library technology that binds a similar but not identical epitope.[14] IK17 Fab was converted to a single-chain fragment containing polyhistidine and hemagglutinin tags, grown on BL21 *Escherichia coli* cells and purified with a nickel column (Qiagen, Valencia, Calif), followed by an anti-hemagglutinin antibody column (Sigma, St Louis, Mo). E06 is a natural murine IgM monoclonal antibody cloned from apolipoprotein E–deficient (apoE$^{-/-}$) mice that binds to

the phosphocholine head group of oxidized, but not native, phospholipids.[15] E06 was purified with high-performance liquid chromatography. All 3 preparations were >99% pure. We rationalized that using 3 distinct oxidation-specific antibodies would provide specific validation of OxLDL as a viable target for molecular imaging of atherosclerotic lesions.

Synthesis and Physical Properties of Micelles

MRI was performed with pegylated gadolinium-labeled micelles as the contrast agent, which were prepared using established thin-film micelle methods (Figure 1).[16,17] In short, 1,2-distearoyl-sn-glycer-3-phosphoethanolamine-n-methoxy(polyethylene glycol-2000) ammonium salt (PEG-DSPE, Avanti Polar Lipids, Alabaster, Ala), GdDTPA-bis(stearyl-amid) (GdDTPA-BSA, Gateway Chemicals, St Louis, Mo), and PEG-malamide-DSPE (Avanti Polar Lipids) were dissolved in chloroform:methanol (molar ratio, 49:50:1) with rhodamine added as a fluorescent label. The solvents were removed under heat and vacuum until a thin film was formed. The film was hydrated in a HEPES buffer (pH 7.0), and the sample was incubated at 65°C until micelles formed.

To generate “targeted” micelles, MDA2, E06, IK17, and nonspecific polyclonal human IgG (Sigma) as an antibody control were modified with S-acetylthioglycolic acid *N*-hydroxysuccinimide ester (SATA) and then covalently linked to the surface of the gadolinium micelles as previously described.[16,17] Untargeted micelles (ie, no antibody present) were used as a no-antibody control.

MDA2 micelles, E06 micelles, IK17 micelles, IgG micelles, and untargeted micelles were characterized with respect to size, relaxation properties, pharmacokinetics, and biodistribution. The size (as hydrated diameter) was determined with dynamic laser light scattering (DSL, Malvern Instruments, Malvern, UK) at 25°C. Longitudinal relaxivities (r1) were determined at 60 MHz and 40°C with a Bruker Minispec (Bruker Medical BmbH, Ettingen, Germany). The relaxation rates (R1) were determined at 6 different concentration levels (0 to 2 mmol/L Gd in HEPES buffer) using an inversion recovery sequence with at least 15 different inversion times. The r1 values were then calculated as the slope associated with a linear fit of gadolinium concentration versus R1. Approximately 50% of the lipid weight was labeled with gadolinium, so there were ≈50 gadolinium ions per micelle.[16]

The attachment of antibodies on micelles was evaluated with a chemiluminescent ELISA[13] and reported as relative light units (RLU) per 100 milliseconds. The antibody micelles were plated directly to microtiter wells, and the presence of MDA2, IK17, and E06 was determined with alkaline phosphatase–labeled goat anti-mouse IgG, goat anti-human Fab, and goat anti-mouse IgM antibodies, respectively.

Animal Models

For imaging studies, a total of 36 apoE$^{-/-}$ mice were used: 8 for untargeted micelles, 8 for MDA2 micelles, 8 for E06 micelles, 3 for IgG micelles, 3 for IK17 micelles, 3 for competitive inhibition studies, and 3 for confocal microscopy studies. Fourteen wild-type (WT) mice were used: 3 for untargeted micelles, 3 for MDA2 micelles, 3 for E06 micelles, 3 for IgG micelles, and 2 for confocal microscopy studies. Both strains of mice were on a

C57BL/6 background. ApoE$^{-/-}$ mice were placed on a high-cholesterol diet (0.2% total cholesterol, Harlan Teklad, Madison, Wis) ad libitum beginning at 6 weeks until 50 to 56 weeks of age. WT mice were maintained on a normal murine diet (Research Diets, Inc, New Brunswick, NJ). The ethics committee at Mount Sinai approved all of the animal experiments.

Pharmacokinetics and Biodistribution of Micelles

The blood half-life and biodistribution of the all micelles were determined in apoE$^{-/-}$ and WT mice after tail vein injection of a 0.075–mmol Gd/kg dose. Blood was drawn over a 96-hour time period (30 apoE$^{-/-}$ mice and 14 WT mice), and gadolinium concentration was determined by inductively coupled plasma mass spectrometry (ICP-MS; Cantest Ltd, Burnaby, British Columbia, Canada). The blood half-life values were calculated from the resultant gadolinium concentration-versus-time curves using standard non-compartmental biexponential pharmacokinetic analysis. The biodistribution of all micelles was determined in the liver, spleen, kidney, heart, lung, and aorta after saline perfusion of the vasculature. Animals were killed over a 24- to 96-hour time interval after injection. Organs were cleaned and weighed, and gadolinium content was determined with ICP-MS. The percent-injected dose (%ID) was determined from the total amount of gadolinium administered and the total gadolinium content in the various organs per gram of wet organ weight.

MRI Studies

The MR efficacy of all micelles was evaluated at 9.4 T with an 89-mm-bore system operating at a proton frequency of 400 MHz (Bruker Instruments, Billerica, Mass). All animals underwent a preinjection MR scan within 24 hours before the administration of micelles. Animals were anesthetized with a 4% isoflurane/O_2 gas mixture (400-cm^3/min initial dose) and maintained with a 1.5% isoflurane/O_2 gas mixture (100-cm^3/min maintenance dose) delivered through a nose cone during tail vein injection of the contrast agents. MRI was performed over a 96-hour time interval after administration of a 0.075–mmol Gd/kg dose of all micelles. No adverse effects were observed during or after micelle administration.

MRI of the abdominal aorta was performed with a T1-weighted black-blood spin-echo sequence (repetition time, 600 ms; echo time, 8.6 ms; flip angle, 30°; number of excitations, 14; field of view, 2.6×2.6 cm) with 16 contiguous 500-μm-thick slices with a microscale in-plane resolution of 101 μm. An inflow saturation band of 3 to 5 mm was used with a slice gap of 3 mm for additional luminal flow suppression. Fourteen signal averages were used for a total imaging time of 36 minutes per scan. A saturation pulse was used to eliminate signal from fat tissue, to better delineate the boundary of the aortic wall, and to minimize chemical shift artifacts. At each time point after injection, the slices were matched to the baseline preinjection scans by using the unique vertebral anatomy and paraspinous muscular anatomy as anatomic landmarks. MRI of the liver was obtained with the sequence described above; however, to minimize breathing motion artifacts, respiratory gating was applied to the T1-weighted black-blood spin-echo sequence. A respiratory sensor was connected to a monitoring and gating system (SA Instruments, Inc, Stony Brook, NY) and placed on the abdomen to monitor the rate and depth of respiration. Because the abdominal aorta was

retroperitoneal, it was stationary in the axial and longitudinal planes relative to the vertebrae, spinal cord, and paraspinous muscles. As a result, no respiratory or cardiac gating was necessary.

To quantitatively analyze the MRI results, signal intensity measurements were obtained from regions of interest on the aortic wall and liver on slices (n>5) exhibiting signal modulation after contrast. The mouse aorta is typically 4 pixels thick, so only 10 to 20 pixels will make up any given region of interest. Because of the small number of pixels involved, the areas associated with the regions of interest were kept constant between the before and after images. Signal intensity measurements of the aortic lumen, muscle, and noise also were obtained for each slice. The percent-normalized enhancement (%NENH) relative to muscle was then determined for the aortic vessel wall and liver according to established methods.[18] The %NENH values reflect the percent change in the contrast-to-noise ratios obtained before and after injection as follows: $\%NENH=[(CNR_{post}/CNR_{pre})-1\times100$, where CNR is the contrast-to-noise ratio defined as $CNR3SNR_{wall}/SNR_{muscle}$ (SNR is the signal-to-noise ratio). CNR_{post} is the CNR value obtained after injection; CNR_{pre} is the CNR value obtained before administration of the micelles.

In Vivo Competitive Inhibition Imaging Studies

To test the specificity of the MDA2 micelles for MDA-lysine epitopes in the vessel wall of $apoE^{-/-}$ mice, in vivo competitive inhibition studies also were performed. Age-matched $apoE^{-/-}$ mice (n=3) were administered 6 mg free MDA2 IV immediately before the administration of MDA2 micelles (0.075 mmol Gd/kg). The MR enhancement of vessel wall and liver was determined and compared with the MR enhancement obtained after the administration of MDA2 micelles (n=3).

Confocal Microscopy

The fluorescently (containing rhodamine [red]) labeled micelles were detected with confocal scanning microscopy (Zeiss LSM 510 META microscope, Carl Zeiss AG, Oberkochen, Germany) in an inverted configuration. The system was equipped with 4 lasers and 3 confocal detectors, and data were captured and analyzed with Zeiss LSM 510 Meta and Image Browser software (Carl Zeiss AG). After the 48-hour postinjection scans, a subgroup (n=3 per group) of animals were killed; the aorta and liver were isolated and frozen in optical cutting temperature compound (Tissue Tek, Sakura Finetech, Tokyo, Japan); and 8-μm frozen sections were cut and fixed in PBS-buffered 4% paraformaldehyde. Sections were rinsed and blocked (PBS containing 0.5% BSA and 5% horse serum) for 45 minutes at room temperature. Macrophages were fluorescently stained with RPE-labeled anti-CD68 primary antibodies (Serotec, Inc, Raleigh, NC), and the nuclei were stained with DAPI. Fluorescently labeled micelles were colocalized with respect to both cell nuclei (blue) and macrophages (green) within the vessel wall and liver. Microscopy sections of the aortas were matched to the MRI slices for comparison and correlation. To evaluate any potential autofluorescence, an age-matched control $apoE^{-/-}$ mouse was killed and perfused, and the aorta was fixed for microscopy.

Assessment of the Association and/or Uptake of Micelles in Macrophages

The confocal microscopy studies suggested that micelles were not just accumulating in atherosclerotic lesions but also were associated with macrophages (see Results). To obtain insights into whether extracellular MDA-LDL influenced this relationship, we incubated micelles with cultured murine macrophages under the 4 following conditions: pre-exposure of macrophages (eighth-generation J774A.1 macrophages) with or without MDA-LDL and pre-exposure of micelles with or without MDA-LDL. To perform these experiments, macrophages were plated into 12-well plates in DMEM containing FCS. In 1 set of these wells, MDA-LDL (5 μg/mL) was added and incubated with macrophages for 24 hours at 37°C. In another set of wells, no MDA-LDL was added, and macrophages were exposed to similar conditions. The wells were then washed in fresh DMEM, and the macrophages were used in the experiments below. In a similar manner, the untargeted micelles (n=2), MDA2 micelles (n=2), IK17 micelles (n=2), IgG micelles (n=2) (all at 1 mmol/L Gd), and saline controls (n=2) were either pre-exposed to MDA-LDL (10 μg/mL) or not pre-exposed to MDA-LDL for 45 minutes at 37°C. The micelles were then incubated with the macrophages (both exposed to MDA-LDL or not exposed to MDA-LDL) for an additional 24 hours at 37°C.

We assessed the association of micelles with macrophages using both quantitative and qualitative measures. The macrophages were gently scraped off the plates, washed in PBS, and split into 2 fractions. One set of cells were used to measure the content of gadolinium per cell as follows: The cells were counted with a bright line counting chamber (Hausser Scientific, Horsham, Pa), and gadolinium content was quantified by ICP-MS and normalized to the number of cells. In the second fraction of cells, a qualitative measure of “uptake” of micelles by the cells was performed with confocal microscopy. For these studies, the cells were fixed on glass slides (4% paraformaldehyde for 10 minutes), and cell nuclei were fluorescently labeled with VectaShield containing 1.5 μg/mL DAPI (Vector Laboratories, Burlingame, Calif) and analyzed by laser scanning confocal microscopy. The spatial relationship of micelles (rhodamine) to macrophage nuclei (DAPI) was then visually assessed.

Statistical Methods

To determine the significance of the MR enhancement at different time points, 1-way ANOVA with Bonferroni’s post hoc multiple-comparison tests was used to compare the %NENH values obtained for the various micelle groups. For all statistical analysis, values of $P<0.05$ were considered significant. The analysis was performed with Number Crunching Statistical System 2001 (NCSS, Kaysville, Utah).

The authors had full access to and take full responsibility for the integrity of the data. All authors have read and agree to the manuscript as written.

Results

Physical Characteristics, Pharmacokinetics, and Biodistribution of Micelles

The size, longitudinal relaxivity, pharmacokinetics, and liver uptake of the various micelles formulations (0.075–mmol Gd/kg dose) were determined in apoE$^{-/-}$ and WT mice (Table 1). The hydrated diameter of the micelles was 14 to 22 nm. The r1 values obtained at 60 MHz were similar in all micelles and were similar to other gadolinium micelles reported in the literature.[16,18] The r1 values obtained for all the micelle formulations tested were at least 3 times greater than the r1 value associated with commercially available Gd-DTPA.[18] In vitro chemiluminescent ELISA confirmed that MDA2, IK17, and E06 were present on the micelles (824±171, 869±134, and 814±152 RLU, respectively, versus 57±27 RLU for untargeted micelles; $P<0.001$).

In WT mice, the blood half-life was ≈1.5 hours for all micelles. However, in apoE$^{-/-}$ mice, the MDA2, IK17, and E06 micelles exhibited significantly longer half-lives than untargeted micelles or IgG micelles ($P<0.001$ for both).

In concert with the longer half-life, MDA2, IK17, and E06 micelles demonstrated greater blood concentration values at 24 hours after injection relative to untargeted micelles and IgG micelles (Figure 2A). The untargeted and IgG micelles were completely cleared from the circulation within 24 hours, but the targeted micelles were still present (but significantly diminished) at 96 hours after injection. Liver, spleen, and kidney uptake peaked at ≈48 hours for the MDA2 micelles, IK17 micelles, and E06 micelles. Liver and spleen uptake over the 96 hours tended to increase for E06 micelles and untargeted micelles. Excretion and/or metabolism of all micelle formulations were observed in the lymphatic system at late time points after injection (maximum value at 48 hours). The targeted micelles also were present in the heart and lung (0.4% and 0.5% of the injected dose at 48 hours after injection for MDA2 micelles and IK17 micelles, respectively) as confirmed by confocal microscopy. Less micelle uptake was observed in these organs for E06, untargeted, and IgG micelles (heart, 0.2%, 0.1%, and 0.2%, respectively; lung, 0.3%, 0.1%, and 0.3%, respectively). Although not all lymph nodes were extracted, the abdominal lymph nodes showed uptake of MDA2 micelles (concentrations were 10±1, 80±16, and 37±5.6 μg/g for 24, 48, and 96 hours after injection, respectively). These results are consistent with the MR images that indicate lymphatic drainage of the micelle formulations. Previous studies have indicated lymphatic involvement with other gadolinium-based micelle platforms.[18]

ICP-MS of apoE$^{-/-}$ mice injected with MDA2 micelles revealed maximum uptake in the aorta at 48 hours after injection (24 hours, 0.30%ID; 48 hours, 0.48%ID; 72 hours, 0.12%ID). Less than 0.03% of the injected dose was found in the aorta of apoE$^{-/-}$ mice after administration of either untargeted or IgG micelles. No gadolinium was detected in the aortas of apoE$^{-/-}$ mice after the administration of either the untargeted or IgG micelles.

MRI Studies

In apoE$^{-/-}$ mice, MDA2, IK17, and E06 micelles demonstrated higher signal (125%, 137%, and 231% NENH, respectively) than adjacent muscle at 72 hours after injection in apoE$^{-/-}$ mice, whereas IgG and untargeted micelles had minimal signal enhancement ($P<0.001$;

Table 2). Consistent with a specific targeting mechanism, preinjection of free MDA2 before intravenous injection of MDA2 micelles resulted in ≈6-fold reduction in %NENH at 72 hours. Interestingly, %NENH in liver also was significantly reduced.

Significant MR signal was observed in the abdominal aorta of apoE$^{-/-}$ mice after administration of MDA2, IK17, and E06 micelles (Figure 3). No significant enhancement was observed after administration of either untargeted micelles or IgG micelles at any time point after injection. The intravenous injection of excess free MDA2 significantly reduced the plaque (and liver [not shown]) enhancement of MDA2 micelles to a level comparable to that of untargeted micelles (Table 2 and Figure 4). Histological confirmation with hematoxylin and eosin staining demonstrated the presence of plaque in arterial segments where imaging was performed (data not shown).

In WT mice, no MR signal enhancement of the arterial vessel wall was observed after administration of the untargeted, MDA2, E06, or IgG micelles at any of the time points tested.

Confocal Microscopy

Confocal microscopy confirmed the association of the MDA2 micelles and E06 micelles (confocal microscopy studies were not done with IK17 micelles) within the arterial vessel wall of apoE$^{-/-}$ mice, as reflected by the red within these cells (Figure 5). Untargeted micelles or IgG micelles were not observed within the arterial vessel wall. There also was evidence of colocalization of rhodamine (micelles) with CD68 staining, consistent with a close association and/or uptake of micelles with macrophages. Confocal imaging of a control apoE$^{-/-}$ aorta indicated no significant red or green autofluorescence within the wall. Liver Kupffer cell uptake of the untargeted, MDA2, E06, and IgG micelles was observed, but hepatocyte parenchymal cell uptake was not observed (data not shown).

Assessment of the In Vitro Association and/or Uptake of Micelles in Macrophages

Figure 6 summarizes the ex vivo macrophage experiment assessing the association and/or uptake of the 4 micelle formulations in J7774A.1 macrophages, both of which were either pre-exposed or not pre-exposed to MDA-LDL. The figure depicts representative images of macrophage nuclei stained with DAPI (blue) and the presence of micelles depicted by rhodamine (red). Below each panel are listed the quantitative ICP-MS data representing gadolinium content from a parallel set of macrophages. The qualitative results indicate that when micelles were pre-exposed to MDA-LDL, there was limited association of micelles with macrophages (column 1). When the macrophages were pre-exposed to MDA-LDL but the micelles were not, MDA2 and IK17 micelles were associated with macrophages (column 2). When the MDA2 and IK17 micelles were preincubated with MDA-LDL but the macrophages were not, there was even greater association of MDA2 and IK17 micelles with macrophages (column 3). Finally, when both macrophages and micelles were pre-exposed to MDA-LDL, the highest association of MDA2 and IK17 micelles with macrophages was noted (column 4). In contrast, minimal association of IgG or untargeted micelles was noted in any condition. No background or autofluorescence was observed in control macrophages (data not shown).

Discussion

The present study demonstrates for the first time that noninvasive imaging of atherosclerotic lesions rich in oxidation-specific epitopes can be accomplished with MRI. Specific targeting of oxidation-specific epitopes was demonstrated using micelles loaded with gadolinium and modified to contain unique oxidation-specific antibodies. Micelles containing no antibody or a nonspecific antibody provided minimal lesion enhancement. Preblocking of available MDA epitopes with free MDA2 abrogated most of the signal enhancement with MDA2 micelles, consistent with an epitope-specific targeting mechanism. Compared with previous imaging approaches with radiolabeled antibodies in rabbits,[13] the image quality, sensitivity, and resolution of this MRI approach are significantly improved. The present experimental validation supports the applicability of in vivo MRI of oxidation-specific epitopes for the identification and quantification of atherosclerotic lesions and potentially the characterization of vulnerable plaque.

The rationale for targeting oxidation-specific epitopes for imaging atherosclerotic plaques, specifically vulnerable plaques, is based on both clinical and experimental data showing intimate relationships of OxLDL with the initiation and progression of atherosclerotic plaques.[2] OxLDL also is associated with destabilization of atherosclerotic plaques as a result of upregulation, synthesis, and release of metalloproteinases from activated macrophages and foam cells.[19] Additionally, OxLDL has been shown both to induce macrophage apoptosis and to hinder phagocytic clearance of the apoptotic cells within lesions.[20] The buildup of apoptotic macrophages and extracellular oxidized lipids and proteins leads to the formation of a necrotic core that may further accelerate plaque rupture.

Recent human studies have shown that vulnerable plaques are enriched in OxLDL, with ≈70-fold higher levels (measured as ng OxLDL per μg apoB) in plaque than blood,[6] and that increased circulating levels of OxLDL are associated with acute coronary syndromes and plaque disruption.[5,21,22] In addition, experimental data from many laboratories have documented that OxLDL is proatherogenic and proinflammatory and mediates many of the underlying mechanisms of plaque growth. For example, in hypercholesterolemic animal models, OxLDL in the vessel wall appears to be present in proportion to the amount of plaque burden.[7,23]

Because OxLDL is immunogenic, antibodies that specifically bind oxidation-specific epitopes may be isolated from animals and humans with atherosclerosis.[24,25] Previous radiotracer studies have shown that the murine antibody MDA2 and the human IK17 Fab localize to lipid-rich, oxidation-rich atherosclerotic lesions in animals.[7,13,14] In fact, in an autoradiographic imaging study in low-density lipoprotein receptor–deficient mice, it was shown that the uptake of ^{125}I-MDA2 accumulated in atherosclerotic plaques in proportion to the presence and extent of OxLDL.[26] Furthermore, during atherosclerosis regression and plaque stabilization, as manifested by loss of macrophages and increased smooth muscle cell and collagen content, ^{125}I-MDA2 accumulation in the plaque was markedly diminished, even before significant geometric plaque regression. In conjunction with loss of imaging signal, there also was immunohistological evidence of the absence of OxLDL from the vessel wall in the early phases of regression and plaque stabilization. ^{99m}Tc-MDA2 also was

shown to provide noninvasive images,[13] but mice cannot be easily imaged noninvasively with radiolabeled antibodies because of a suboptimal plaque-to-blood ratio and inadequate resolution of nuclear techniques in these models. However, other nuclear imaging approaches targeting macrophage/foam cells, matrix metalloproteinases, and apoptosis have promising roles in detecting vulnerable plaques.[27] The present study, showing significantly enhanced image quality, suggests that MRI may provide enhanced sensitivity to image important changes in atherosclerotic lesions during atherosclerosis progression and regression.

The importance of the specific in vivo uptake of the targeted micelles was demonstrated with competitive inhibition studies showing that specific antibody targeting of the MDA2 micelles into atherosclerotic plaque and macrophages could be abrogated by preinjection of free MDA2. The data are consistent with saturation of available MDA-lysine epitopes, thereby limiting MR enhancement of the arterial vessel wall. Consistent with this mechanism, excess MDA2 also limited uptake of MDA2 micelles in the liver, which is enriched in Kupfer cells and likely enriched in oxidation-specific epitopes. Because prior studies using radiolabeled MDA2 suggested a strong correlation between ^{125}I-MDA2 plaque uptake and OxLDL content, it is hypothesized that MR molecular imaging probes targeting OxLDL may allow in vivo evaluation of therapeutic interventions that promote the efflux of OxLDL epitopes from these lesions.[26] This has implications in not only imaging oxidation-rich lesions but also having the ability to follow their natural history or with therapeutic interventions.

The targeted micelles (MDA2, IK17, and E06) exhibited a significantly longer circulating half-life than the untargeted or IgG micelles. However, this was noted only in apoE$^{-/-}$ mice, which are expected to have higher levels of circulating OxLDL in the blood and vessel wall.[23] It is possible that binding of these micelles to circulating OxLDL may have reduced blood clearance. The prolonged plasma residence time of targeted micelles may have allowed more time for greater accumulation of the micelles within the arterial wall and greater uptake by macrophages. The safety implications of these observations need to be studied in the future.

The biodistribution and confocal microscopy results show significant accumulation of the targeted micelles within atherosclerotic lesions with peak aortic wall concentration at 24 hours but optimal enhancement at 72 hours. In addition, colocalization of targeted micelles with macrophages in atherosclerotic plaques was noted. The in vitro experiments suggested that extracellular MDA-LDL may mediate this interaction. This may be due to micelle binding to the macrophage surface and/or being specifically taken up by macrophages. This may be facilitated by uptake of MDA-LDL micelle complexes by macrophage scavenger receptors (there was an molar excess of MDA epitopes compared with MDA2 in this in vitro experiment). Furthermore, induction of macrophage apoptosis by exposure to MDA-LDL with subsequent expression of oxidation-specific epitopes leading to enhanced uptake,[28] macropinocytosis,[29] and other undefined mechanisms may also be important pathways of micelle uptake by macrophages. Uptake of MDA2 micelles by macrophage-foam cells through the Fc portion of MDA2 is not likely to be the dominant pathway because micelles coated with IK17, which lacks an Fc region, had an uptake similar to that of MDA2

micelles. Furthermore, limited uptake in macrophages was noted by micelles coated with nonspecific IgG, which has an Fc region. The biodistribution results also suggest that cells associated with the reticuloendothelial system are involved in the excretion of both targeted and untargeted micelles. Interestingly, MDA2 micelles exhibited an initial high uptake in the lymphatic system, which would be expected to be enriched in oxidized lipids.

Other lipid-based molecular imaging platforms have been used previously to target plaque macrophages.[30] These platforms use either anti-CD204 micelles targeting macrophage scavenger receptors or modified native high-density lipoprotein–targeted micelles, but using different amphipliles and attachment methods (POPC lipids, Tween80 surfactant, and avidin-biotin bridging). Relative to the anti-CD204 micelles, the MDA2, IK17, and E06 micelles exhibited smaller hydrated mean diameters (102 versus 22 nm) and longer half-lives. From this variation in size and pharmacokinetics, different plaque uptake would be expected. Anti-CD204 micelles exhibited greater background enhancement (%NENH >60% at 0.0338 mmol Gd/kg) after injection of untargeted micelles and more diffuse uptake within the arterial wall relative to micelles targeted to oxidation-specific epitopes.[18,30] Furthermore, the anti-CD204 micelle arterial vessel wall enhancement peaked at 24 hours, whereas the targeted micelles in the present study had prolonged arterial vessel wall enhancement that reached a maximum value at 72 hours after injection (125% to 231%), suggesting more specific uptake mechanisms. Additional studies must be performed with the same lipid platform to accurately compare the MRI efficacy of macrophage scavenger receptors and OxLDL targeting.

Study Limitations

Compared with other mouse models, apoE$^{-/-}$ mice have atherosclerotic lesions most similar to vulnerable plaques in patients. However, we did not specifically image vulnerable plaques in this study. Additionally, immune responses to the use of antibodies and the mechanisms of macrophage uptake and the excretion pathways of these targeted micelles need to be evaluated in future studies.

Conclusions

The present study demonstrates a novel method for noninvasively imaging oxidation-specific epitopes within atherosclerotic lesions that builds on the wealth of basic and clinical data on the role of oxidation in mediating cardiovascular disease. If validated and translated to humans, this imaging approach may provide valuable tools to noninvasively detect, quantify, and monitor atherosclerosis in general and potentially image vulnerable plaques locally.

Acknowledgments

The authors would like to thank high school students Alexander M. Saeboe (Somers High School, Somers, NY), Sheena Hakimian, and Jessica Mounessa (both from Great Neck High School, Long Island, NY) who participated in the preparation of micelles.

Sources of Funding

This investigation was supported in part by the Fondation Leducq (Drs Witztum and Tsimikas), an unrestricted grant from Atherotope, Inc (Dt Tsimikas), NIH/NHLBI R01 HL071021 and R01 HL078667 grants (Dr Fayad), and American Heart Association Grant Award 0430127N (Dr Shaw).

References

1. Fuster V, Moreno PR, Fayad ZA, Corti R, Badimon JJ. Atherothrombosis and high-risk plaque, part I: evolving concepts. J Am Coll Cardiol. 2005; 46:937–954. [PubMed: 16168274]
2. Glass CK, Witztum JL. Atherosclerosis: the road ahead. Cell. 2001; 104:503–516. [PubMed: 11239408]
3. Virmani R, Burke AP, Farb A, Kolodgie FD. Pathology of the vulnerable plaque. J Am Coll Cardiol. 2006; 47:C13–C18. [PubMed: 16631505]
4. Waxman S, Ishibashi F, Muller JE. Detection and treatment of vulnerable plaques and vulnerable patients: novel approaches to prevention of coronary events. Circulation. 2006; 114:2390–2411. [PubMed: 17130356]
5. Ehara S, Ueda M, Naruko T, Haze K, Itoh A, Otsuka M, Komatsu R, Matsuo T, Itabe H, Takano T, Tsukamoto Y, Yoshiyama M, Takeuchi K, Yoshikawa J, Becker AE. Elevated levels of oxidized low density lipoprotein show a positive relationship with the severity of acute coronary syndromes. Circulation. 2001; 103:1955–1960. [PubMed: 11306523]
6. Nishi K, Itabe H, Uno M, Kitazato KT, Horiguchi H, Shinno K, Nagahiro S. Oxidized LDL in carotid plaques and plasma associates with plaque instability. Arterioscler Thromb Vasc Biol. 2002; 22:1649–1654. [PubMed: 12377744]
7. Tsimikas S, Shortal BP, Witztum JL, Palinski W. In vivo uptake of radiolabeled MDA2, an oxidation-specific monoclonal antibody, provides an accurate measure of atherosclerotic lesions rich in oxidized LDL and is highly sensitive to their regression. Arterioscler Thromb Vasc Biol. 2000; 20:689–697. [PubMed: 10712392]
8. Tsimikas S, Aikawa M, Miller FJ Jr, Miller ER, Torzewski M, Lentz SR, Bergmark C, Heistad DD, Libby P, Witztum JL. Increased plasma oxidized phospholipid:apolipoprotein B-100 ratio with concomitant depletion of oxidized phospholipids from atherosclerotic lesions after dietary lipid-lowering: a potential biomarker of early atherosclerosis regression. Arterioscler Thromb Vasc Biol. 2007; 27:175–181. [PubMed: 17082490]
9. Tsimikas S, Brilakis ES, Miller ER, McConnell JP, Lennon RJ, Kornman KS, Witztum JL, Berger PB. Oxidized phospholipids, Lp (a) lipoprotein, and coronary artery disease. N Engl J Med. 2005; 353:46–57. [PubMed: 16000355]
10. Tsimikas S. Oxidized low-density lipoprotein biomarkers in atherosclerosis. Curr Atheroscler Rep. 2006; 8:55–61. [PubMed: 16455015]
11. Cai J, Hatsukami TS, Ferguson MS, Kerwin WS, Saam T, Chu B, Takaya N, Polissar NL, Yuan C. In vivo quantitative measurement of intact fibrous cap and lipid-rich necrotic core size in atherosclerotic carotid plaque: comparison of high-resolution, contrast-enhanced magnetic resonance imaging and histology. Circulation. 2005; 112:3437–3444. [PubMed: 16301346]
12. Desai MY, Lima JA. Imaging of atherosclerosis using magnetic resonance: state of the art and future directions. Curr Atheroscler Rep. 2006; 8:131–139. [PubMed: 16510047]
13. Tsimikas S, Palinski W, Halpern SE, Yeung DW, Curtiss LK, Witztum JL. Radiolabeled MDA2, an oxidation-specific, monoclonal antibody, identifies native atherosclerotic lesions in vivo. J Nucl Cardiol. 1999; 6:41–53. [PubMed: 10070840]
14. Shaw PX, Hörkkö S, Tsimikas S, Chang MK, Palinski W, Silverman GJ, Chen PP, Witztum JL. Human-derived anti-oxidized LDL autoantibody blocks uptake of oxidized LDL by macrophages and localizes to atherosclerotic lesions in vivo. Arterioscler Thromb Vasc Biol. 2001; 21:1333–1339. [PubMed: 11498462]
15. Hõrkkõ S, Bird DA, Miller E, Itabe H, Leitinger N, Subbanagounder G, Berliner JA, Friedman P, Dennis EA, Curtiss LK, Palinski W, Witztum JL. Monoclonal autoantibodies specific for oxidized phospholipids or oxidized phospholipid-protein adducts inhibit macrophage uptake of oxidized low-density lipoproteins. J Clin Invest. 1999; 103:117–128. [PubMed: 9884341]

16. Mulder WJ, Koole R, Brandwijk RJ, Storm G, Chin PT, Strijkers GJ, de Mello DC, Nicolay K, Griffioen AW. Quantum dots with a paramagnetic coating as a bimodal molecular imaging probe. Nano Lett. 2006; 6:1–6. [PubMed: 16402777]
17. Torchilin VP, Lukyanov AN, Gao Z, Papahadjopoulos-Sternberg B. Immunomicelles: targeted pharmaceutical carriers for poorly soluble drugs. Proc Natl Acad Sci U S A. 2003; 100:6039–6044. [PubMed: 12716967]
18. Briley-Saebo KC, Amirbekian V, Mani V, Aguinaldo JG, Vucic E, Carpenter D, Amirbekian S, Fayad ZA. Gadolinium mixed micelles: effect of the amphiphile on in vitro and in vivo efficacy in apolipoprotein E knockout mouse models of atherosclerosis. Magn Reson Med. 2006; 56:1336–1346. [PubMed: 17089381]
19. Rajavashisth TB, Xu XP, Jovinge S, Meisel S, Xu XO, Chai NN, Fishbein MC, Kaul S, Cercek B, Sharifi B, Shah PK. Membrane type 1 matrix metalloproteinase expression in human atherosclerotic plaques: evidence for activation by proinflammatory mediators. Circulation. 1999; 99:3103–3109. [PubMed: 10377072]
20. Chang MK, Binder CJ, Miller YI, Subbanagounder G, Silverman GJ, Berliner JA, Witztum JL. Apoptotic cells with oxidation-specific epitopes are immunogenic and proinflammatory. J Exp Med. 2004; 200:1359–1370. [PubMed: 15583011]
21. Tsimikas S, Bergmark C, Beyer RW, Patel R, Pattison J, Miller E, Juliano J, Witztum JL. Temporal increases in plasma markers of oxidized low-density lipoprotein strongly reflect the presence of acute coronary syndromes. J Am Coll Cardiol. 2003; 41:360–370. [PubMed: 12575961]
22. Tsimikas S, Lau HK, Han KR, Shortal B, Miller ER, Segev A, Curtiss LK, Witztum JL, Strauss BH. Percutaneous coronary intervention results in acute increases in oxidized phospholipids and lipoprotein(a): short-term and long-term immunologic responses to oxidized low-density lipoprotein. Circulation. 2004; 109:3164–3170. [PubMed: 15184281]
23. Tsimikas S, Palinski W, Witztum JL. Circulating autoantibodies to oxidized LDL correlate with arterial accumulation and depletion of oxidized LDL in LDL receptor-deficient mice. Arterioscler Thromb Vasc Biol. 2001; 21:95–100. [PubMed: 11145939]
24. Binder CJ, Shaw PX, Chang MK, Boullier A, Hartvigsen K, Horkko S, Miller YI, Woelkers DA, Corr M, Witztum JL. The role of natural antibodies in atherogenesis. J Lipid Res. 2005; 46:1353–1363. [PubMed: 15897601]
25. Shaw PX, Hörkkö S, Chang MK, Curtiss LK, Palinski W, Silverman GJ, Witztum JL. Natural antibodies with the T15 idiotype may act in atherosclerosis, apoptotic clearance, and protective immunity. J Clin Invest. 2000; 105:1731–1740. [PubMed: 10862788]
26. Torzewski M, Shaw PX, Han KR, Shortal B, Lackner KJ, Witztum JL, Palinski W, Tsimikas S. Reduced in vivo aortic uptake of radiolabeled oxidation-specific antibodies reflects changes in plaque composition consistent with plaque stabilization. Arterioscler Thromb Vasc Biol. 2004; 24:2307–2312. [PubMed: 15528482]
27. Davies JR, Rudd JH, Weissberg PL, Narula J. Radionuclide imaging for the detection of inflammation in vulnerable plaques. J Am Coll Cardiol. 2006; 47:C57–C68. [PubMed: 16631511]
28. Chang MK, Bergmark C, Laurila A, Hörkkö S, Han KH, Friedman P, Dennis EA, Witztum JL. Monoclonal antibodies against oxidized low-density lipoprotein bind to apoptotic cells and inhibit their phagocytosis by elicited macrophages: evidence that oxidation-specific epitopes mediate macrophage recognition. Proc Natl Acad Sci U S A. 1999; 96:6353–6358. [PubMed: 10339591]
29. Ide M, Kuwamura M, Kotani T, Sawamoto O, Yamate J. Effects of gadolinium chloride (GdCl(3)) on the appearance of macrophage populations and fibrogenesis in thioacetamide-induced rat hepatic lesions. J Comp Pathol. 2005; 133:92–102. [PubMed: 15964588]
30. Amirbekian V, Lipinski MJ, Briley-Saebo KC, Amirbekian S, Aguinaldo JG, Weinreb DB, Vucic E, Frias JC, Hyafil F, Mani V, Fisher EA, Fayad ZA. Detecting and assessing macrophages in vivo to evaluate atherosclerosis noninvasively using molecular MRI. Proc Natl Acad Sci U S A. 2007; 104:961–966. [PubMed: 17215360]

CLINICAL PERSPECTIVE

Oxidized low-density lipoprotein plays a key role in the initiation, progression, and destabilization of atherosclerotic plaques and is present in macrophages and the lipid pool. Development of sensitive molecular imaging probes that target oxidation-specific epitopes in the vessel wall may allow in vivo detection of plaque vulnerability, which can be used as an index of clinical risk. Because of its submillimeter resolution, magnetic resonance imaging has emerged as a promising technique for both direct assessment of plaque burden and evaluation of plaque composition, particularly in large vessels. In the present study, we demonstrated the magnetic resonance imaging efficacy of micelles loaded with gadolinium and unique human (IK17) or murine antibodies (MDA2 and E06), which recognize oxidation-specific epitopes, to image atherosclerotic lesions noninvasively. This approach was highly specific for targeting oxidation-specific epitopes as documented by several control experiments in which injection of unlabeled antibodies prevented MR lesion enhancement. Magnetic resonance imaging with these oxidized low-density lipoprotein–targeted micelles demonstrated excellent image quality of oxidation-rich atherosclerotic lesions. The present study describes a novel method for noninvasively imaging oxidation-specific epitopes within atherosclerotic lesions that builds on the wealth of basic and clinical data on the role of oxidation in mediating cardiovascular disease. If validated and translated to humans, this imaging approach may provide valuable tools to noninvasively detect, quantify, and monitor atherosclerosis in general and potentially image vulnerable plaques locally.

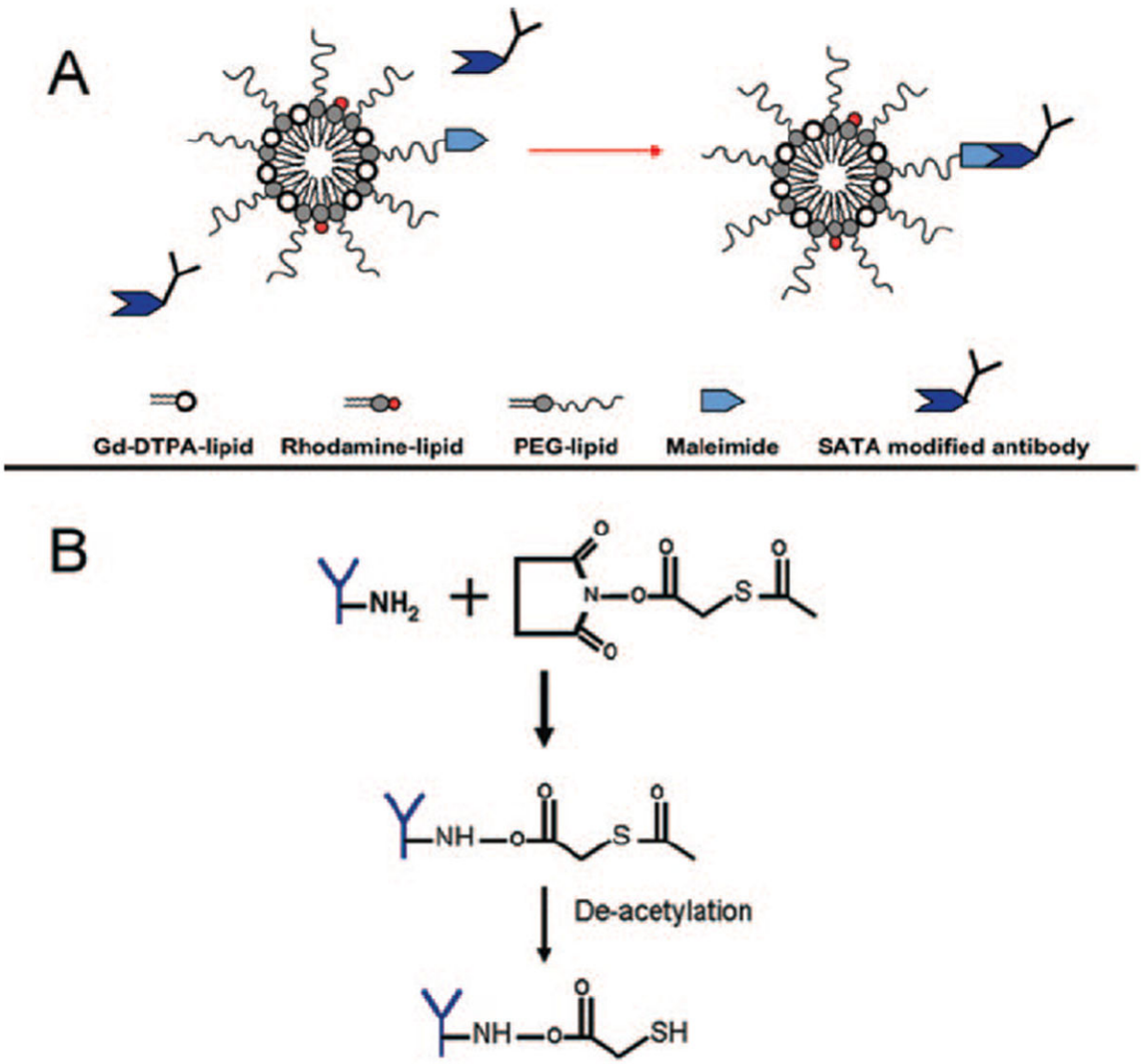

Figure 1.

Schematic of S-acetythioglycolic acid N-hydroxysuccinimide ester (SATA) attachment to antibodies, micelle composition, and attachment of antibodies to micelles. A, Composition of the micelles. B, Modification of the antibodies with the SATA linker to facilitate attachment to the micelles via the maleimide moiety.

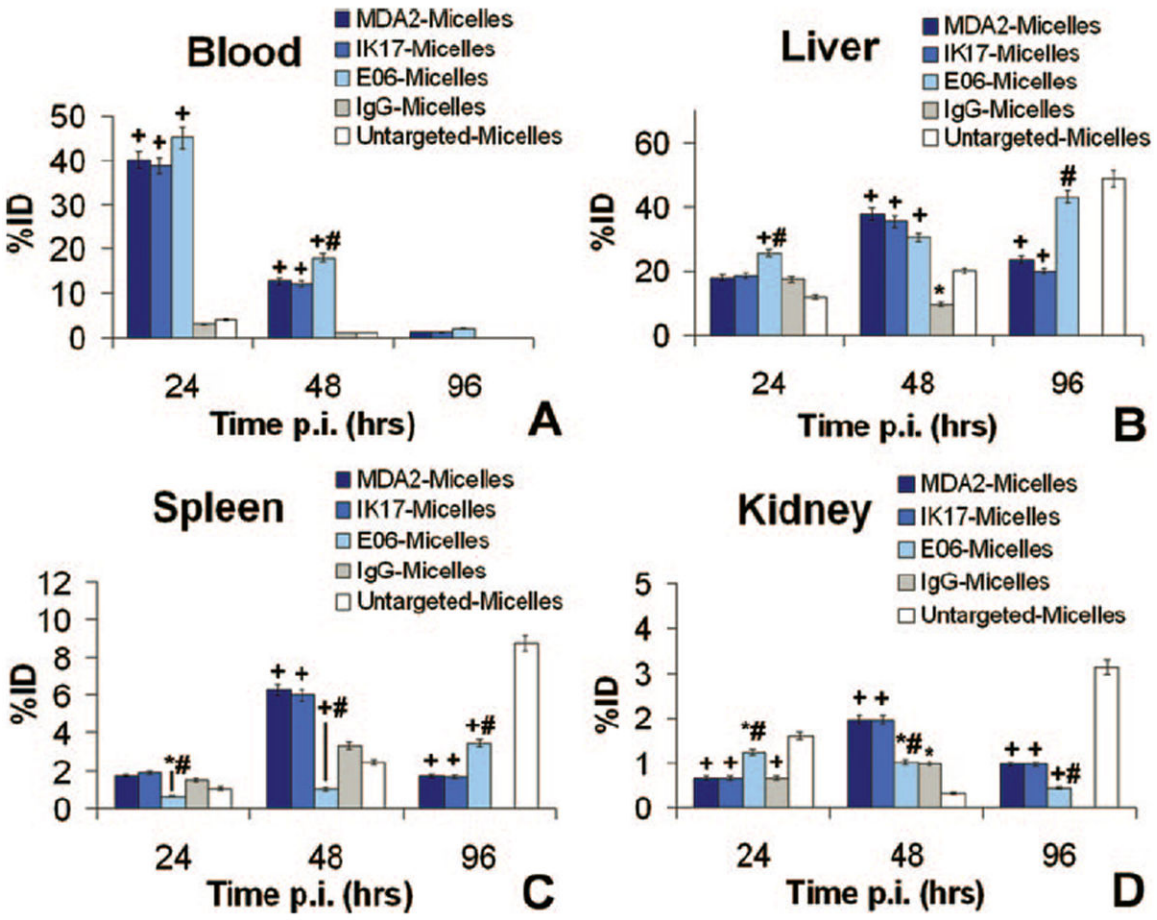

Figure 2.

Biodistribution of MDA2, IK17, E06, IgG, and untargeted micelles (0.075–mmol Gd/kg dose) at 24, 48, and 98 hours after injection (p.i.) in apoE$^{-/-}$ mice. The %ID in blood (A), liver (B), kidney (C), and spleen (D). +P<0.001, *P<0.05, differences between MDA2, IK17, E06, and IgG micelle and untargeted micelles at each time point. #P<0.05, differences between MDA2, IK17, and E06 micelles at each time point.

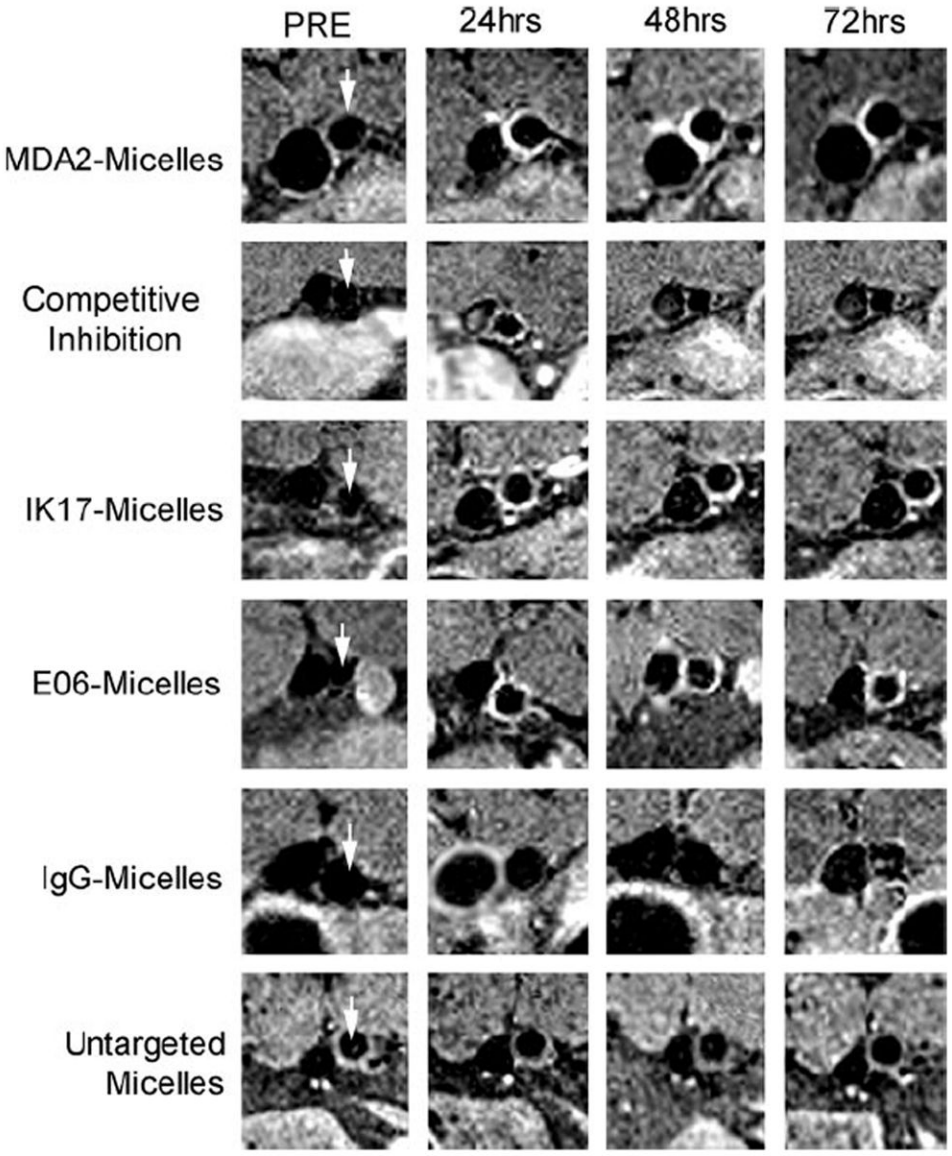

Figure 3.

Representative abdominal aorta (arrows) enhancement in apoE$^{-/-}$ mice as a function of time after injection of 0.075–mmol Gd/kg micelles. The vessel to the left of the aorta is the inferior vena cava (IVC). Although arterial flow was saturated to allow delineation of the arterial wall, some enhancement in the IVC may be observed because of flow artifacts.

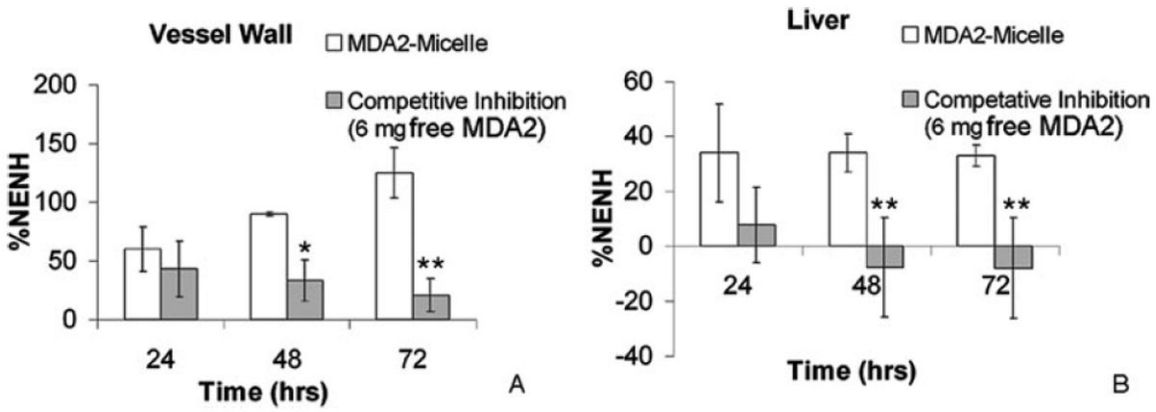

Figure 4.

Comparison of the quantitative uptake (%NENH) of MDA2 micelles in the arterial vessel wall (A) and liver (B) before and after administration of excess free MDA2. *P<0.05, **P<0.001, differences between groups.

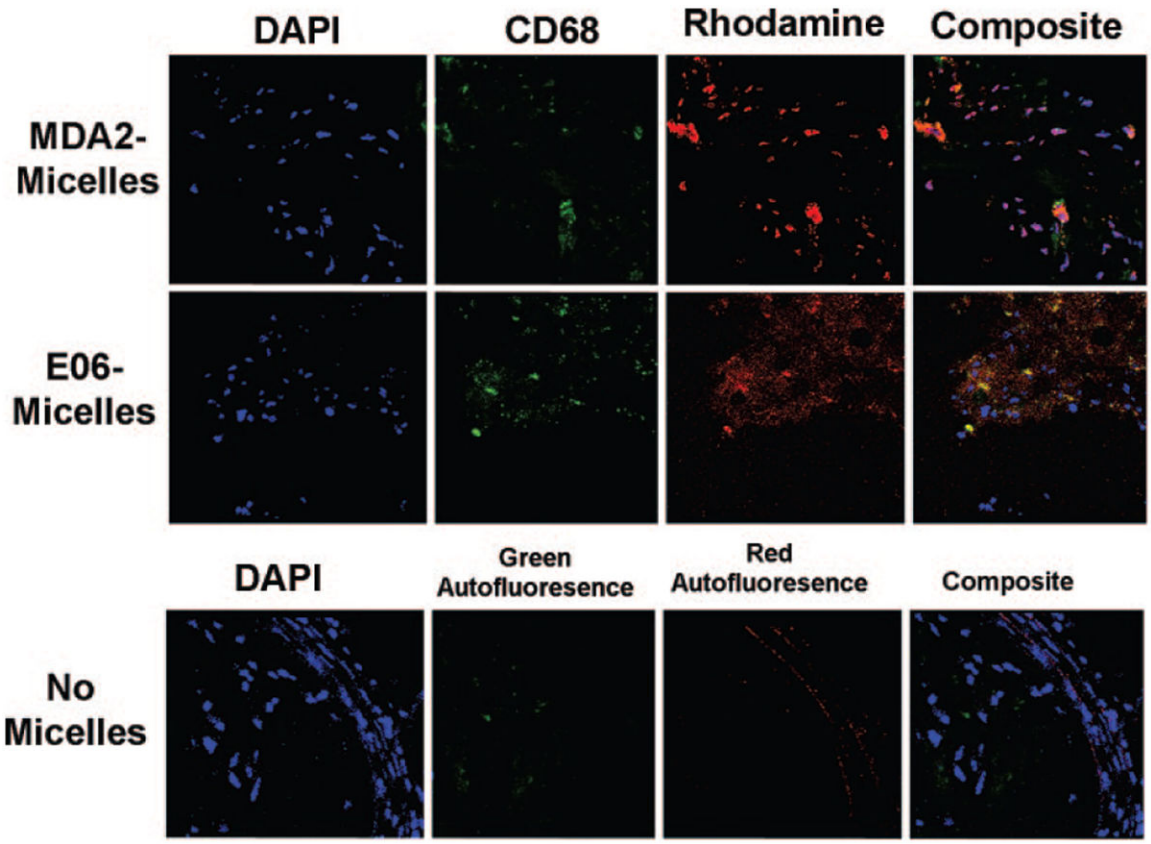

Figure 5.

Confocal microscopy (×63) of apoE$^{-/-}$ mouse aortic atherosclerotic plaque after administration of MDA2 and E06 micelles demonstrating nuclei (blue), macrophages (green), and micelles (red). Bottom, An atherosclerotic plaque from an apoE$^{-/-}$ mouse not injected with micelles stained with DAPI showing the absence of significant autofluorescence (×40).

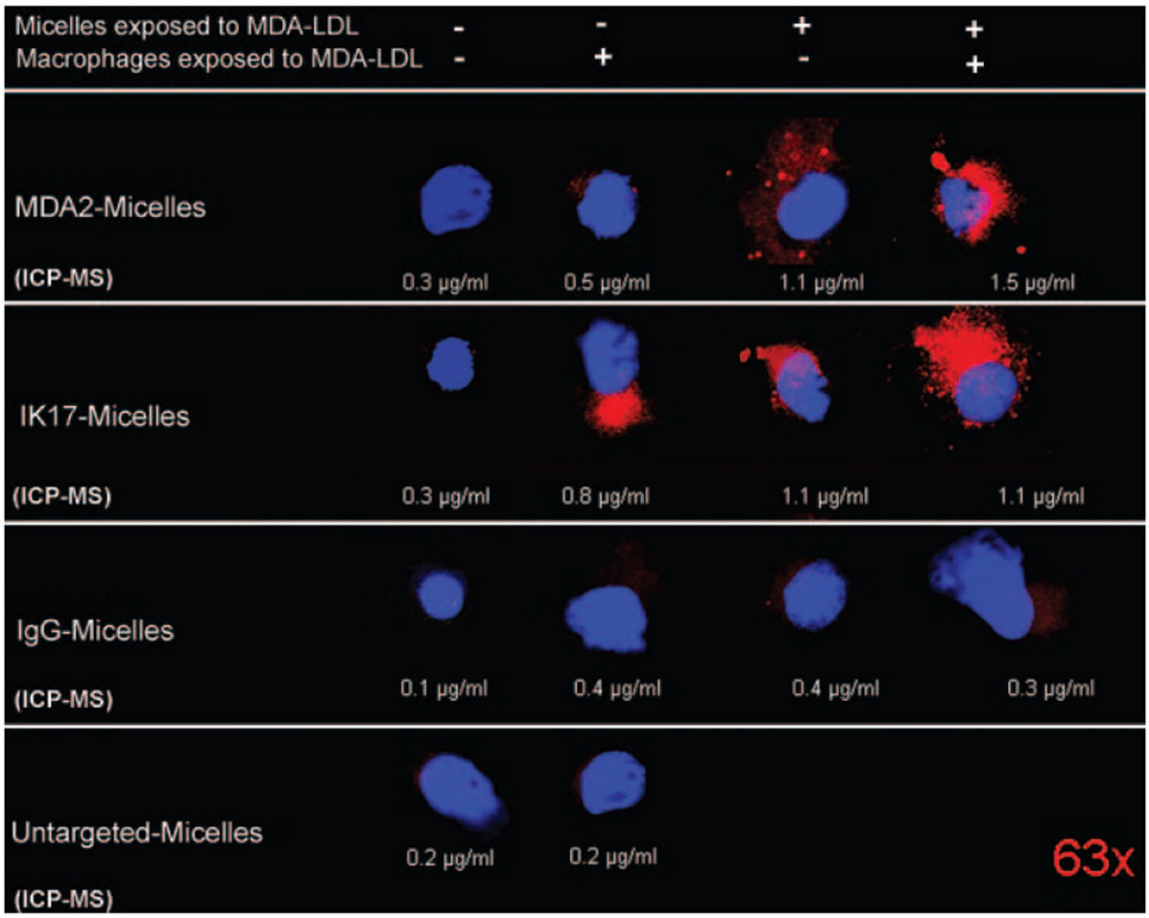

Figure 6.

Confocal microscopy (×63) showing the association of micelles with macrophages in in vitro experiments. Macrophages and micelles were either exposed (+) or not exposed (−) to MDA-LDL before being mixed together in cell culture. Red (rhodamine) represents the presence of micelles; blue (DAPI), macrophage nuclei. The numbers under each panel represent gadolinium content measured by ICP-MS normalized to total cell number.

Table 1

Physical and Chemical Properties and Pharmacokinetics of Micelles

Formulation	Size, nm	r1 at 60 MHz, $s^{-1} \cdot mmol/L^{-1}$	Blood Half-Life, h		%ID in Liver of ApoE$^{-/-}$ Mice at 24 h
			ApoE$^{-/-}$ Mice	WT Mice	
MDA2 micelles	22±2	9.3	14.3*	1.7	18±4
IK17 micelles	16±3	10.5	16.5*	1.8	18±4
E06 micelles	16±3	10.8	20.1*	1.7	32±2
IgG micelles	16±4	10.4	1.4	1.3	18±3
Untargeted micelles	14±2	11.6	1.5	1.5	12±3

* $P<0.001$ vs WT mice.

Table 2

%NENH of the Abdominal Aortic Wall and Liver Relative to Muscle as a Function of Micelle Formulation and Time After Injection in ApoE$^{-/-}$ Mice

	Time After Injection, h		
	24	**48**	**72**
%NENH vessel wall of ApoE$^{-/-}$ mice			
MDA2 micelles (n=8)	60±9*	90±3*	125±22*
E06 micelles (n=8)	93±54*	88±7*	231±40*
IK17 micelles (n=3)	82±40*	95±49*	138±35*
IgG micelles (n=3)	3±33	−8±9	−0.6±29
Untargeted micelles (n=8)	20±18	2±20	15±10
Competitive inhibition (n=3)	43±24	33±18	20±15
%NENH in liver of ApoE$^{-/-}$ mice			
MDA2 micelles (n=8)	34±18	34±7	33±4
E06 micelles (n=8)	39±10	40±9	49±17
IK17 micelles (n=3)	27±6	42±10	38±6
IgG micelles (n=3)	27±10	10±9†	−4±4‡
Untargeted micelles (n=8)	38±5	42±5	39±10
Competitive inhibition (n=3)	8±3†	−8±8*	−8±8†

* $P<0.001$,

† $P<0.01$,

‡ $P<0.05$ vs untargeted micelles.